

Experimental implementation of phase triplicator gratings in a spatial light modulator

Shang Gao (高尚)^{1*}, María del Mar Sánchez-López^{1,2**}, and Ignacio Moreno^{1,3}

¹Instituto de Bioingeniería, Universidad Miguel Hernández, Elche 03202, Spain

²Departamento de Física Aplicada, Universidad Miguel Hernández, Elche 03202, Spain

³Departamento de Ciencia de Materiales, Óptica y Tec. Electrónica, Universidad Miguel Hernández, Elche 03202, Spain

*Corresponding author: sgao@umh.es

**Corresponding author: mar.sanchez@umh.es

Received July 6, 2023 | Accepted September 28, 2023 | Posted Online February 21, 2024

In this work, we compare different methods for implementing a triplicator, a phase grating that generates three equi-intense diffraction orders. The design with optimal efficiency features a continuous phase profile, which cannot be easily reproduced, and is typically affected by quantization. We compare its performance with binary and sinusoidal phase profiles. We also analyze the effect of quantizing the phase levels. Finally, a random approach is adopted to eliminate the additional harmonic orders. In all cases, a liquid-crystal-on-silicon spatial light modulator is employed to experimentally verify and compare the different approaches.

Keywords: diffraction gratings; phase modulation; triplicator; spatial light modulators.

DOI: [10.3788/COL202422.020501](https://doi.org/10.3788/COL202422.020501)

1. Introduction

Diffraction gratings of evenly distributed intensity among a number of diffraction orders, also called fan-out elements, are interesting for developing beam splitters and optical array illuminators. They were developed by the end of the 20th century, when the emergence of micro-optics technology made their fabrication possible^[1]. One popular initial approach was the Dammann grating^[2], which has a binary phase profile where the period is divided into different transition points^[3]. Other approaches based on multilevel^[4] or continuous^[5] phase profiles were developed later.

One particular case is the triplicator, a 1×3 fan-out diffraction grating that produces three equi-intense diffraction orders. Gori *et al.*^[6] derived the analytical solution for the phase-only design with optimal diffraction efficiency that yields 92.6% of the light intensity in the 0th and ± 1 st orders. However, this solution features a continuous phase profile, which is difficult to properly reproduce, and is typically affected by quantization effects, which become more relevant as the period of the gratings gets reduced. Nevertheless, optimal phase triplicator gratings have been demonstrated with spatial light modulators (SLMs)^[7], with geometric-phase metasurfaces^[8], and with structured liquid crystals^[9]. The optimal triplicator design has recently received renewed attention for applications in telecommunications^[10] and for the physical implementation of trifocal diffractive intraocular lenses^[11,12].

In this work, we investigate the optimum triplicator design and the effect of quantizing the phase levels. Theoretical and experimental results for different phase triplicator designs are presented, where we use a liquid-crystal-on-silicon (LCOS) SLM to experimentally verify their properties. We compare the optimum design with the binary phase profile, a very simple alternative that provides an efficiency of 86.4%, and with the sinusoidal profile, which reaches 90.0% efficiency. In addition, we present a random multiplexing approach with much less efficiency but free of unwanted higher-order harmonics that affect the former designs. Let us remark that we consider in all cases scalar triplicators, i.e., we do not consider vectorial diffraction gratings^[13,14], which can reach 100% efficiency but are polarization-sensitive.

The paper is organized as follows. After this introduction, Section 2 describes the experimental setup. Section 3 reviews the Fourier theory and describes the different grating designs and their experimental implementation. Section 4 presents the study in terms of the number of phase levels, and Section 5 discusses the random approach. Conclusions are given in Section 6.

2. Methods: Experimental System

The experimental setup is shown in Fig. 1. A He–Ne laser beam of 632.8 nm wavelength is expanded through a spatial filter (SF)

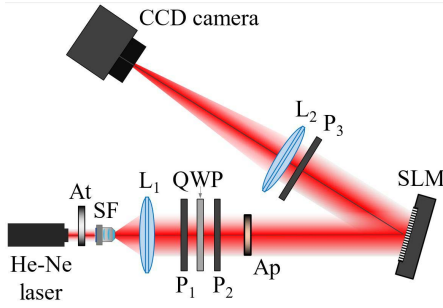


Fig. 1. Experimental setup. At, variable attenuator; P_1 , P_2 , P_3 , linear polarizers; L_1 , L_2 , convergent lenses; QWP, quarter-wave plate; SF, spatial filter; Ap, circular aperture.

and collimated by a lens (L_1). An attenuator (At) adjusts the input intensity. Then, a system composed by a linear polarizer P_1 and a quarter-wave plate (QWP) with its neutral axis oriented 45° relative to P_1 is used to generate circularly polarized light. Therefore, the output intensity after linear polarizer P_2 is constant, regardless of its orientation. This way we can illuminate the LCOS-SLM with an arbitrary polarization orientation while keeping a constant intensity. A circular aperture allows for the adjustment of the beam diameter. The LCOS-SLM employed (Thorlabs Exulus) is a phase-only display with full HD resolution, comprising $1920 \text{ pixels} \times 1080 \text{ pixels}$ of $6.4 \mu\text{m}$ size.

First, the phase modulation of the display was calibrated using a standard technique^[15]. It shows a linear phase modulation versus the addressed gray level and reaches a maximum 2π phase depth. To display the phase diffraction gratings, the transmission axis of P_2 is set parallel to the SLM LC director, so the input light beam is fully modulated. Let us note that some works^[14] exploited the possibility of not aligning the input polarizer parallel to the LC director, such that the nonmodulated portion of the input beam contributes to the zeroth order. This results in a polarizing diffraction grating. Here, we consider pure scalar phase-only gratings. The linear polarizer P_3 is also set parallel to the LCOS director. Finally, the light beam reflected from the SLM is focused by a lens (L_2) on a CCD camera (Basler sca1390-17 fc, with 1390×1038 square pixels of $4.65 \mu\text{m}$ size), where the diffraction pattern is captured.

3. Methods: Fourier Analysis of Phase Gratings

The paraxial Fourier optics domain is considered, where a scalar phase-only diffraction grating with period p can be expanded as a Fourier series^[16],

$$g(x) = e^{i\varphi(x)} = \sum_{m=-\infty}^{+\infty} c_m e^{im2\pi x/p}, \quad (1)$$

whose coefficients are given by

$$c_m = \frac{1}{p} \int_{-p/2}^{+p/2} g(x) e^{-im2\pi x/p} dx. \quad (2)$$

Each term $e^{im2\pi x/p}$ in Eq. (1) represents a tilted plane wave that generates a diffraction order with index m . The intensity of each order is given by $I_m = |c_m|^2$. Some classical designs are the blazed grating, a linear phase profile producing a modulo 2π single $e^{\pm i2\pi x/p}$ term, which renders a single diffraction order with 100% efficiency, and the binary grating with π phase shift, which generates equally intense ± 1 st orders and cancels the 0th order.

The triplicator diffraction grating is defined to provide three equally intense diffraction orders $I_0 = I_1 = I_{-1}$ with the maximum possible efficiency given by

$$\eta_{0\pm 1} = I_0 + I_1 + I_{-1}. \quad (3)$$

3.1. Binary phase grating profile

Let us first regard the binary phase grating. This grating is interesting not only because it is simpler to fabricate; it also serves to calibrate the phase modulation in SLMs^[17]. The Fourier coefficients [Eq. (2)] for this grating are given by

$$c_0 = \frac{1}{2} (e^{i\varphi} + 1), \quad (4a)$$

$$c_{m \neq 0} = \frac{1}{2} (e^{i\varphi} - 1) \text{sinc}\left(\frac{m}{2}\right), \quad (4b)$$

where $\text{sinc}(x) = \sin(\pi x)/(\pi x)$, and φ denotes the phase difference between the two levels in the grating. Thus, the intensity of the 0th and ± 1 st orders is

$$I_0 = |c_0|^2 = \frac{1}{2} (1 + \cos \varphi), \quad (5a)$$

$$I_{\pm 1} = |c_{\pm 1}|^2 = \frac{2}{\pi^2} (1 - \cos \varphi). \quad (5b)$$

Figure 2(a) shows the theoretical (lines) and experimental (dots) normalized intensity of the 0th and ± 1 st orders of a binary phase grating as a function φ . Figure 2(b) shows camera captures of some diffraction patterns. When $\varphi = \pi$, the 0th order is canceled and the ± 1 st orders reach $I_{\pm 1} = 40.5\%$. The rest of the energy is diffracted to other higher orders, $m = \pm 3, \pm 5, \dots$. However, note the two curves' intersections in Fig. 2(a) at $\varphi = 0.639\pi$ or $\varphi = 1.361\pi$, where $I_0 = I_{\pm 1} = 0.288$, thus rendering a triplicator with $\eta_{0\pm 1} = 86.4\%$ efficiency.

The experiments in Fig. 2 confirm this result. We encode gratings with a period of $p = 64$ pixels, to minimize the pixel cross talk that degrades gratings with short periods^[18]. The images in Fig. 2(b) are deliberately saturated to make the higher orders clearly visible.

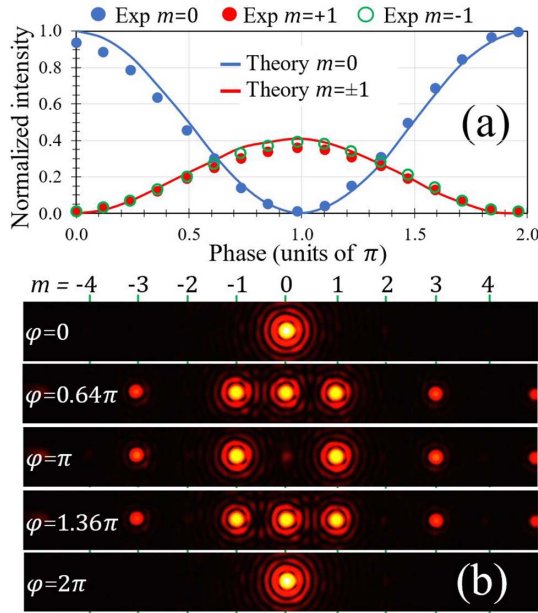


Fig. 2. Binary phase grating. (a) Normalized intensity of diffraction orders versus phase level; (b) experimental diffraction patterns for different phase values.

3.2. Sinusoidal phase grating profile

Another classical phase-only grating often found in the literature is the sinusoidal phase profile given by

$$\varphi(x, a) = \pi + a\pi \cdot \cos\left(\frac{2\pi x}{p}\right). \quad (6)$$

Here the phase varies sinusoidally with x , with an elongation $\pm a\pi$, around a central value that we chose, π , so that the phase profile $\varphi(x, a)$ is within the range $[0, 2\pi]$ for values $a \in [0, 1]$. For this profile, the Fourier coefficients are given by $I_n = |J_n(a\pi)|^{2[16]}$, where $J_n(x)$ are the Bessel functions,

$$J_n(x) = \frac{1}{2\pi} \int_{-\pi}^{\pi} e^{i(x \sin \beta - n\beta)} d\beta. \quad (7)$$

Figure 3(a) shows the theoretical intensity of the zeroth, first, and second diffraction orders as a function of parameter a , as well as the measured normalized intensity.

For low parameter values, most of the light remains on the zeroth order. When the curves for the zeroth and first orders intersect, a triplicator grating is obtained, a situation that occurs for $a = 0.457$, for which the total efficiency is $\eta_{0\pm1} = 90.0\%$. Figure 3(b) shows the experimental diffraction pattern for various values of a . The result for $a = 0.457$ confirms the generation of triplicator, with three equi-intense central orders. However, most of the noncontributing light is concentrated on the ± 2 nd orders. As parameter a continues grow, light is diffracted onto higher orders. The zeroth order vanishes for $a = 0.765$.

Note that the sinusoidal phase profile in Eq. (6) is continuous. Since the SLM is a pixelated device, it can only display discrete

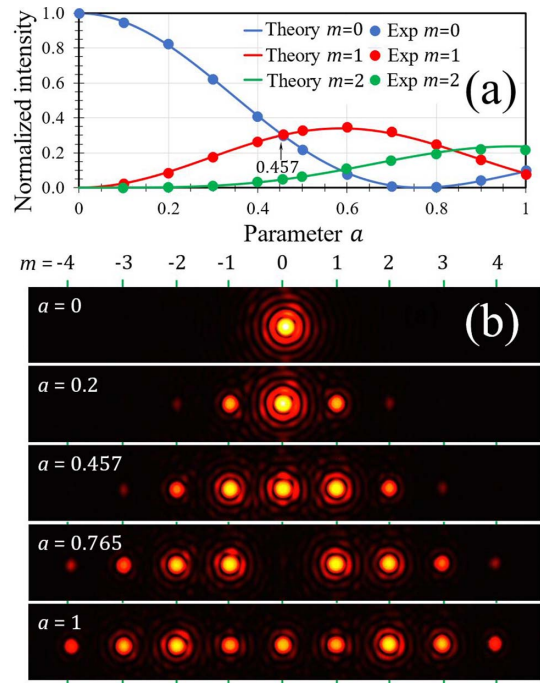


Fig. 3. Sinusoidal phase grating. (a) Normalized intensity versus parameter a ; (b) experimental diffraction patterns.

steps. However, since we encode the gratings with $p = 64$ pixels per period, this quantization does not significantly affect the results.

3.3. Gori's optimum triplicator profile

In 1998 Gori *et al.*^[6] derived the phase grating profile providing a triplicator with optimal efficiency, whose solution was demonstrated to be

$$\varphi(x, a) = \pi + \arctan \left[a \cdot \cos\left(\frac{2\pi x}{p}\right) \right], \quad (8)$$

where again we add π to have phase values in the range $[0, 2\pi]$. This solution maximizes $\eta_{0\pm1}$ [Eq. (3)] and provides intensities at the zeroth and first diffraction orders given by

$$I_0 = \frac{4}{\pi^2} [K(-a^2)]^2, \quad (9a)$$

$$I_{\pm 1} = \frac{4}{\pi^2 a^2} [E(-a^2) - K(-a^2)]^2, \quad (9b)$$

where $K(m)$ and $E(m)$ are the complete elliptic integrals of the first and second kind, respectively. The optimum triplicator is retrieved for $a = 2.65$.

Parameter a in Eq. (8) controls the phase profile and the relative intensity between the 0th and ± 1 st orders. Figure 4(a) shows the phase profiles for three values of a . Note the profile is sinusoidal for $a = 1$, but it tends to the binary profile for large values of a . For very low values, the phase modulation is reduced,

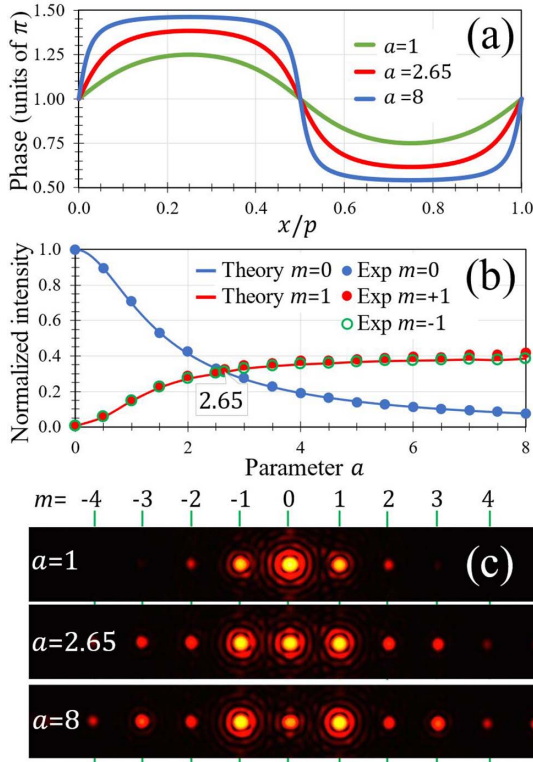


Fig. 4. Gori's optimum triplicator. (a) Phase profile for $a = 1$, $a = 2.65$, and $a = 8$; (b) theoretical and experimental normalized intensity of the 0th and ± 1 st orders versus a ; (c) experimental diffraction patterns for different values of a .

reaching a uniform phase in the limit $a \rightarrow 0$ that renders only the 0th order. The normalized intensity of the 0th and ± 1 st orders, Eq. (9), is depicted in Fig. 4(b), together with the experimental measurements. To our knowledge, these results are the first experimental verification of Gori's profile versus a . Figure 4(c) shows some captures of the diffraction pattern. Again, the gratings are displayed with 64 pixels per period; thus the quantization effect is negligible. For $a = 2.65$, the expected optimum triplicator is obtained. We measure an experimental efficiency $\eta_{0\pm 1} = 94.7\%$, in agreement with the theoretical value in Ref. [6].

4. Quantized Profiles

The continuous profile of Gori's triplicator is ill-reproduced in a pixelated SLM if the grating's period p is not large enough. Multilevel phase gratings were designed, for instance, in Ref. [4], and a four-level phase triplicator was calculated in Ref. [19]. In this section, we analyze phase diffraction gratings with a discrete number of phase levels. But, having in mind their implementation with a pixelated SLM, the phase levels must be regarded equispaced, as shown in Fig. 5, where we consider N different phase levels ($\varphi_0, \varphi_1, \dots, \varphi_{N-1}$) located at positions (x_0, x_1, \dots, x_{N-1}) within one period (p). The length of each

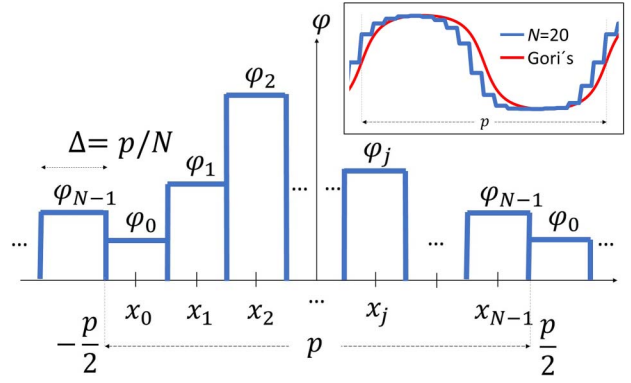


Fig. 5. Quantized phase profile. Inset, for $N = 20$ versus Gori's.

phase segment is $\Delta = p/N$, which corresponds to a single pixel in the SLM. This grating can be described as

$$g(x) = \sum_{j=0}^{N-1} e^{i\varphi_j} \cdot \text{rect}\left(\frac{x - x_j}{\Delta}\right), \quad (10)$$

where each pixel is assigned a phase φ_j within a rectangle of width Δ , $j = 0, 1, \dots, N-1$ and where the center of each pixel is given by

$$x_j = \frac{p}{2} \cdot \left(\frac{2j+1}{N} - 1\right). \quad (11)$$

The rectangle function in Eq. (10) is defined as $\text{rect}(x) = 1$ if $|x| \leq 1/2$ and zero elsewhere.

The Fourier coefficients $c_m(N)$ in Eq. (2) are now

$$c_m = \frac{1}{N} \text{sinc}\left(\frac{m}{N}\right) \sum_{j=0}^{N-1} e^{i\varphi_j} e^{-im2\pi x_j/p}, \quad (12)$$

and the corresponding intensity of the diffraction orders is

$$I_m = \frac{\text{sinc}^2\left(\frac{m}{N}\right)}{N^2} \times \left\{ N + \sum_{j \neq k=0}^{N-1} 2 \cos\left[\varphi_j - \varphi_k - \frac{2\pi m(j-k)}{N}\right] \right\}. \quad (13)$$

By computing Eq. (13), for each value of N we seek for the phases φ_j that provide a triplicator response. In all cases, we find numerical solutions with a perfect intensity uniformity of the three diffraction orders and select the one with the maximum efficiency $\eta_{0\pm 1}$. Figure 6(a) shows $\eta_{0\pm 1}$ versus N , and Fig. 6(b) plots the intensity of the second orders ($\eta_{\pm 2} = I_2 + I_{-2}$) and third orders ($\eta_{\pm 3} = I_3 + I_{-3}$). These curves reveal that, for low odd values $N = 3$ and $N = 5$, the efficiency is lower than that of the binary triplicator, $\eta_{0\pm 1} = 86.4\%$. For $N = 3$ the 3rd orders vanish because the phase profile converges to a binary grating with 1/3 fill factor^[20]. For $N = 4$, the solution is equivalent to the binary case but two pixels are assigned to each level.

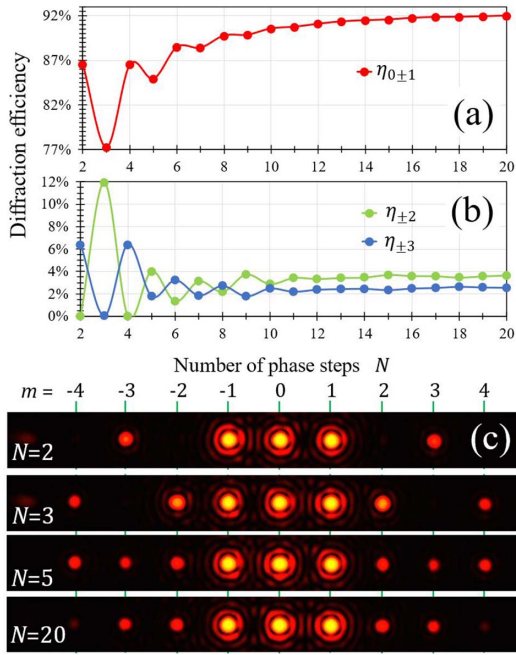


Fig. 6. Calculated diffraction efficiency of the quantized triplicator as a function of N . (a) $\eta_{0\pm 1}$; (b) $\eta_{\pm 2}$ and $\eta_{\pm 3}$; (c) experimental diffraction patterns with $N = 2, 3, 5$, and 20 .

Note that this is different from the four-phases solution proposed in Ref. [19], which considers different lengths of the grating period for each phase level; thus it is not possible to implement it with four equispaced pixels per period. Only when the number of levels reaches $N = 6$ is the efficiency of the binary triplicator surpassed, and then it slowly increases with N . We simulate up to $N = 20$, for which $\eta_{0\pm 1} = 92\%$, very close to that of Gori's triplicator and whose quantized phase profile approaches the continuous one (inset, Fig. 5). Figure 6(c) shows some experimental captures of these quantized triplicators; they all feature the three central equi-intense orders, but also a number of higher orders.

5. Random Approach

All the previous approaches have shown a good efficiency in the generation of the three central orders, but the remaining intensity is concentrated in unwanted higher harmonic orders. Depending on the application, these orders are not desired and are sometimes referred to as noise orders^[21]. In this section, we adopt a random multiplexing approach invented by Davis and Cottrell^[22] and further exploited to implement phase gratings^[23]. This approach consists in randomly addressing to each pixel the phase of one of the different phase functions to be multiplexed. The large number of pixels nowadays available in modern SLM devices makes this approach interesting^[24].

Figure 7 shows the gray-level pattern addressed to the SLM and the corresponding diffraction pattern. The three first rows in Fig. 7 show, respectively, the result when a uniform phase, a

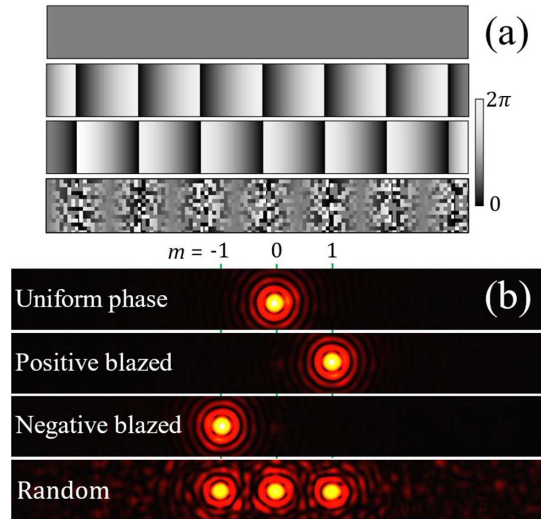


Fig. 7. (a) Illustration of the gray-level image addressed to the SLM and (b) the corresponding experimental diffraction patterns for a uniform phase, a positive and a negative blazed gratings, and the random triplicator generated by randomly addressing to 4×4 macropixels the phase of either the uniform grating or that of the positive or the negative blazed grating.

positive blazed grating, and a negative blazed grating are displayed on the SLM. In the three cases, a unique diffraction order is generated. Therefore, an effective multiplexing of these three phase functions renders the triplicator, without the production of parasite higher orders, a property that has been recently exploited in vortex fork gratings^[25]. The experimental results for the random approach are presented in the last capture of Fig. 7(b). The corresponding gray-level function addressed to the LCOS-SLM [last row in Fig. 7(a)] shows how the phase values are randomly selected among the values of the positive blazed grating, of the negative blazed grating, or of the uniform phase. If the random selection is made at each individual pixel, the result is affected by the pixel cross talk caused by the fringing effect in the SLM, which was demonstrated to generate additional zeroth order and higher harmonics when encoding high spatial frequencies^[26]. To minimize this effect, the randomness is addressed to larger macropixels consisting of 4×4 individual pixels. The triplicator is now successfully obtained with a complete suppression of the additional harmonic orders. However, the price to pay is a lower diffraction efficiency, which is approximately one-third of that of the optimum triplicator^[23]. Light not contributing to the 0th order and ± 1 st orders appears as a background speckle-type noise that limits the efficiency. In these figures, the input intensity was increased by a factor of about 3 in comparison with Figs. 3, 4, and 6.

6. Conclusions

In conclusion, our work has explored how to implement scalar phase-only triplicators, fan-out elements generating three equi-intense diffraction orders. We have compared different designs

and used a phase-only LCOS-SLM to experimentally verify their properties and analyze the difficulties in their implementation.

Gori's optimum triplicator design^[6] has the highest efficiency ($\eta_{0\pm1} = 92.6\%$). We experimentally verified the intensities of the 0th and 1st diffraction orders of this optimum design and compared it to the binary and sinusoidal profiles. We found that the binary grating ($N = 2$) is a feasible option, with an efficiency $\eta_{0\pm1} = 86.4\%$, and it is quite an isolated triplicator (it does not exhibit ± 2 nd orders). We considered quantized phase profiles and performed a numerical search of the phase-level values that provide the triplicator with the highest efficiency for steps from $N = 2$ to $N = 20$. Notably, the performance of the binary phase grating is not surpassed until $N = 6$ phase levels are available. Finally, we implemented a random approach that selectively takes the phase values among two blazed gratings and a constant phase. This approach is interesting because it eliminates the unwanted diffraction orders, although at the cost of reducing the diffraction efficiency. We believe the results of this study are interesting for recent implementations of phase triplicators in biological and telecommunications applications.

Acknowledgements

This work was supported by the Ministerio de Ciencia e Innovación, Spain (PID2021-126509OB-C22) and Generalitat Valenciana (CIAICO/2021/276).

References

1. J. N. Mait, "Design of binary-phase and multiphase Fourier gratings for array generation," *J. Opt. Soc. Am. A* **7**, 1514 (1990).
2. H. Dammann and E. Klotz, "Coherent optical generation and inspection of two dimensional periodic structures," *Opt. Acta* **24**, 505 (1977).
3. C. Zhou and L. Liu, "Numerical study of Dammann array illuminators," *Appl. Opt.* **34**, 5961 (1995).
4. S. J. Walker and J. Jahns, "Array generation with multilevel phase gratings," *J. Opt. Soc. Am. A* **7**, 1509 (1990).
5. L. A. Romero and F. M. Dickey, "The mathematical theory of laser beam-splitting gratings," *Prog. Opt.* **54**, 319 (2010).
6. F. Gori, M. Santarsiero, S. Vicalvi, *et al.*, "Analytical derivation of the optimum triplicator," *Opt. Commun.* **157**, 13 (1998).
7. A. Cofré, P. García-Martínez, A. Vargas, *et al.*, "Vortex beam generation and other advanced optics experiments reproduced with a twisted-nematic liquid-crystal display with limited phase modulation," *Eur. J. Phys.* **38**, 014005 (2017).
8. M. Yannai, E. Maguid, A. Faerman, *et al.*, "Spectrally interleaved topologies using geometric phase metasurfaces," *Opt. Express* **26**, 31031 (2018).
9. D. Marco, M. M. Sánchez-López, A. Cofré, *et al.*, "Optimal triplicator design applied to a geometric phase vortex grating," *Opt. Express* **27**, 14472 (2019).
10. F. Frezza, M. Marciniak, and L. Pajewski, "The optimum-efficiency beam multiplier for an arbitrary number of output beams and power distribution," *J. Telecommun. Inf. Technol.* **3**, 94 (2017).
11. F. Vega, M. Valentino, F. Rigato, *et al.*, "Optical design and performance of a trifocal sinusoidal diffractive intraocular lens," *Biomed. Opt. Express* **12**, 3338 (2021).
12. Y. Xing, Y. Liu, K. Li, *et al.*, "Approach to the design of different types of intraocular lenses based on an improved sinusoidal profile," *Biomed. Opt. Express* **14**, 2821 (2023).
13. J. Tervo and J. Turunen, "Paraxial-domain diffractive elements with 100% efficiency based on polarization gratings," *Opt. Lett.* **25**, 785 (2000).
14. C. R. Fernández-Pousa, I. Moreno, J. A. Davis, *et al.*, "Polarizing diffraction-grating triplicators," *Opt. Lett.* **26**, 1651 (2001).
15. A. Vargas, R. Donoso, M. Ramírez, *et al.*, "Liquid crystal retarder spectral retardance characterization based on a Cauchy dispersion relation and a voltage transfer function," *Opt. Rev.* **20**, 378 (2013).
16. J. W. Goodman, *Introduction to Fourier Optics*, 3rd ed. (Roberts & Company, 2005).
17. G. Lu, Z. Zhang, S. Wu, *et al.*, "Simple method for measuring phase modulation in liquid crystal televisions," *Opt. Eng.* **33**, 3018 (1994).
18. I. Moreno, M. M. Sánchez-López, J. A. Davis, *et al.*, "Simple method to evaluate the pixel crosstalk caused by fringing field effect in liquid-crystal spatial light modulators," *J. Europ. Opt. Soc.* **17**, 27 (2021).
19. R. Borghi, F. Frezza, and L. Pajewski, "Optimization of a four-level triplicator using genetic algorithms," *J. Electromagn. Waves Appl.* **15**, 1161 (2001).
20. A. Martínez, M. M. Sánchez-López, and I. Moreno, "Phasor analysis of binary diffraction gratings with different fill factors," *Eur. J. Phys.* **28**, 805 (2007).
21. S. Buehling, H. Schimmel, and F. Wyrowski, "Challenges in industrial applications of diffractive beam splitting," *Proc. SPIE* **5182**, 123 (2003).
22. J. A. Davis and D. M. Cottrell, "Random mask encoding of multiplexed phase-only and binary phase-only filters," *Opt. Lett.* **19**, 496 (1994).
23. J. Alberio and I. Moreno, "Grating beam splitting with liquid crystal adaptive optics," *J. Opt.* **14**, 075704 (2012).
24. R. Li, Y. Ren, T. Liu, *et al.*, "Generating large topological charge Laguerre-Gaussian beam based on 4K phase-only spatial light modulator," *Chin. Opt. Lett.* **20**, 120501 (2022).
25. H. Hu, X. Zhang, H. Li, *et al.*, "Self-standing quasi-random-dots fork gratings for single-order diffraction," *J. Appl. Phys.* **132**, 223105 (2022).
26. J. A. Davis, E. D. Wolfe, I. Moreno, *et al.*, "Encoding complex amplitude information onto phase-only diffractive optical elements using binary phase Nyquist gratings," *OSA Contin.* **4**, 896 (2021).